Contribution from the Institut für Anorganische Chemie der Universität Bern, CH-3000 Bern 9, Switzerland

# Luminescence Properties of $CsNiX_3$ and $CsMg_{1-x}Ni_xX_3$ (X = Cl, Br)

Christian Reber and Hans U. Güdel*

*Received August 24, 1985*

Single-crystal luminescence and absorption spectra as well as luminescence decay times of $CsNiCl_3$, $CsNiBr_3$, $CsMg_{1-x}Ni_xCl_3$, and $CsMg_{1-x}Ni_xBr_3$ were measured between 10 K and room temperature. The first excited state, $^3T_{2g}$, shows a large trigonal splitting in absorption. Some fine structure in the luminescence spectrum was analyzed in terms of electronic origins and vibronic side bands. The temperature dependence of the decay times and luminescence intensities in the doped compounds were used to characterize the radiative and radiationless deactivation of a single $Ni^{2+}$ center in the diluted samples. In $CsNiCl_3$ and $CsNiBr_3$ the presence of excitation energy transfer was established.

## 1. Introduction

$CsNiCl_3$, $CsNiBr_3$, and their magnesium analogues are well-known examples of quasi-one-dimensional compounds.[1] The structure consists of chains of trigonally elongated face-sharing $NiX_6^{4-}$ octahedra running parallel to the $c$ axis. The space group is $P6_3/mmc$.[1-4] It has been shown that $CsNiCl_3$ and $CsNiBr_3$ undergo phase transitions to an antiferromagnetically ordered state at 4.4 and 14 K, respectively.[5] Exchange effects have also been observed in their absorption spectra.[6,7] According to these results luminescence from the $^3T_{2g}$ state could be expected in the near-infrared region, but the luminescence properties of these compounds have not been explored. In the $Ni^{2+}$-doped lattices MgO,[8] $KZnF_3$,[8] and $MgF_2$,[8] $^3T_{2g} \rightarrow {}^3A_{2g}$ emission has been observed, and the first broad-band-tunable solid-state laser material was $Mg_{1-x}Ni_xF_2$.[9] During the last years the interest in near-infrared laser devices as drivers for fiber optics systems has increased.[10] Luminescence spectroscopy turned out to be a valuable tool for laser material research as well as for fundamental studies. The method allows one to determine static properties of a system, e.g. electronic and vibrational energies, and symmetries and equilibrium geometries of the emitting states, as well as dynamical processes, e.g. nonradiative multiphonon relaxation or transfer of excitation energy. In this work we report single-crystal luminescence spectra, luminescence decay time measurements, and near-infrared absorption spectra of the title compounds between 10 K and room temperature in section 3. The emphasis of the discussion in section 4 is on the lowest energy $^3A_{2g} \leftrightarrow {}^3T_{2g}$ ($O_h$ notation) transitions.

## 2. Experimental Section

Single crystals of the doped compounds $CsMg_{1-x}Ni_xX_3$ and the pure alkali metal nickel halides $CsNiX_3$ (X = Cl, Br) were grown by using the Bridgman technique. The host lattices were prepared by fusing equimolar amounts of CsCl (Merck Suprapur, dried at 300 °C) and $MgCl_2$ (Ventron, 99%, molten under HCl gas) to obtain $CsMgCl_3$ and CsBr (Merck Suprapur, dried at 300 °C) and $MgBr_2$ (Great Western Inorganics, 99.99%, molten under HBr gas) for $CsMgBr_3$. Then 1-5 mol % of $NiCl_2$ (CERAC/PURE) and $NiBr_2$ (CERAC/PURE), respectively, were added and the single crystals obtained in a Bridgman furnace at 650-700 °C with a pulling rate of 0.03 mm/min. As this technique is a zone-refining method, there is a concentration gradient along the crystal boule with the lowest $Ni^{2+}$ concentration on top.

The procedure for the pure compounds was similar: Stoichiometric amounts of the respective cesium and nickel halides were heated in quartz ampules to 750 °C for 12 h, and then single crystals were grown in a Bridgman furnace at 770 °C ($CsNiCl_3$) and 720 °C ($CsNiBr_3$) with a pulling rate of 0.03 mm/min. All the starting materials and products were checked for purity by powder X-ray diffraction.

The crystals cleave easily parallel to the $c$ axis. Samples suitable for $\sigma$ ($\vec{E} \perp c$) and $\pi$ ($\vec{E} \parallel c$) spectroscopic measurements were therefore cleaved from the boules with a razor blade. They were checked for depolarization under a polarizing microscope.

Absorption spectra were recorded on a Cary 17 spectrophotometer equipped with a pair of Glan-Taylor prisms. The crystals were cooled in a closed-cycle helium cryostat (Air Products CSA-202G). Luminescence spectra were measured as follows: The light of a Xe lamp (Varian VIX 150 UV), filtered with a $CuSO_4$ solution and a heat absorption filter (Schott KG3), was used to excite the sample, which was cooled by means of the helium gas flow-tube technique. The emitted radiation was dispersed by a 0.75-m monochromator (Spex 1702) and detected with a cooled PbS cell (77 K, OptoElectronics OE-20-02(X)) in conjunction with a chopper and a lock-in amplifier (PAR 186A).

For the measurement of luminescence decay curves the samples were excited with the 514.5-nm line of a pulsed Ar laser (Spectra Physics 166). The luminescence was detected through a cutoff filter (Schott RG 1000) with an InAs photodiode (Judson Infrared J12A, operated at 300 K) using a preamplifier (PAR 115) and a boxcar integrator (PAR 162 with PAR 164 gated integrator).

For all the experiments data acquisition was performed with a Tektronix 4052A microcomputer.

## 3. Spectroscopic Results

The low-temperature absorption spectra of the title compounds in the region of d-d excitations have previously been reported.[6,7] Our own measurements differ from those in ref 6 and 7 only in detail. In the following we will focus on the lowest energy transitions $^3A_{2g} \leftrightarrow {}^3T_{2g}$ ($O_h$ notation). The corresponding low-temperature absorption and emission spectra for $CsMg_{1-x}Ni_xCl_3/CsNiCl_3$ and $CsMg_{1-x}Ni_xBr_3/CsNiBr_3$ are shown in Figures 1 and 2, respectively. The overall absorption spectra of the diluted and concentrated samples are not significantly different in this spectral region. The emission spectra are disturbed by atmospheric water absorption at about 5100 $cm^{-1}$ although the monochromator was purged with dry nitrogen gas. This absorption is due to a combination of the bending and asymmetrical stretching mode of the $H_2O$ molecule. The luminescence spectrum of the doped chloride compound shows considerable vibronic structure whereas in the absorption spectrum only a very weak origin was detected, as can be seen in Figure 3. The origins of absorption and luminescence coincide. The fine structure is interpreted in section 4.1.

The $^3A_{2g} \rightarrow {}^3T_{2g}$ absorption bands are split and much broader than the luminescence bands. This indicates that transitions to the two trigonal components of $^3T_{2g}$ are observed, while in emission only luminescence from the lowest energy component is present. The Stokes shift was determined by using the lower energy absorption maximum and the maximum of the luminescence band. The resulting values are 1800 and 2150 $cm^{-1}$ for $CsMg_{1-x}Ni_xCl_3$ and $CsMg_{1-x}Ni_xBr_3$, respectively. The intensity of the luminescence bands shows a strong temperature dependence between 10 K and room temperature, as can be seen from Figure 4 for the doped as well as the pure alkali metal nickel halides. The luminescence of the pure materials is quenched at 100 K, whereas the diluted samples luminesce up to much higher temperature. In both the pure and diluted materials the bromide luminescence quenching occurs at lower temperature.

(1) Achiwa, N. *J. Phys. Soc. Jpn.* **1969**, *27*, 561.
(2) Stucky, G. D.; D'Agostinho, S.; McPherson, G. L. *J. Am. Chem. Soc.* **1966**, *88*, 4828.
(3) McPherson, G. L.; Kistenmacher, T. J.; Stucky, G. D. *J. Chem. Phys.* **1970**, *52*, 815.
(4) McPherson, G. L.; McPherson, A. M.; Atwood, J. L. *J. Phys. Chem. Solids* **1980**, *41*, 495.
(5) Witteveen, J. H. T.; Van Veen, J. A. R. *J. Phys. Chem. Solids* **1974**, *35*, 337.
(6) McPherson, G. L.; Stucky, G. D. *J. Chem. Phys.* **1972**, *37*, 3780.
(7) Ackerman, J.; Holt, E. M.; Holt, S. L. *J. Solid State Chem.* **1974**, *9*, 279.
(8) Iverson, M. V.; Sibley, W. A. *J. Lumin.* **1979**, *20*, 311.
(9) Johnson, L. F.; Dietz, R. E.; Guggenheim, H. J. *Phys. Rev. Lett.* **1963**, *11*, 318.
(10) Pappalardo, R. G. In "Spectroscopy of Solid State Laser Materials". Di Bartolo, B., Ed.; Plenum Press: New York; in press.

0020-1669/86/1325-1196$01.50/0 

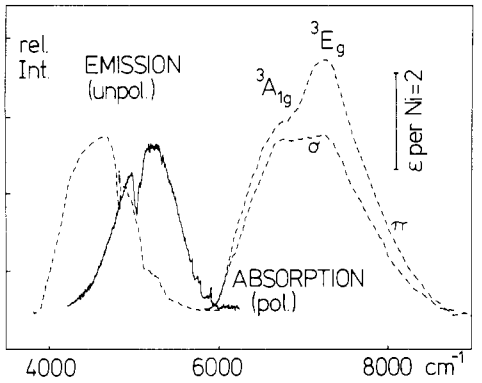


**Figure 1.** Emission spectra of $CsMg_{1-x}Ni_xCl_3$ ($x < 0.01$, $T = 13$ K, solid line) and $CsNiCl_3$ ($T = 15$ K, dashed line) and absorption spectrum of $CsNiCl_3$ ($T = 12$ K, dashed line). The instrumental artifact denoted by i is due to a silica lens absorption.

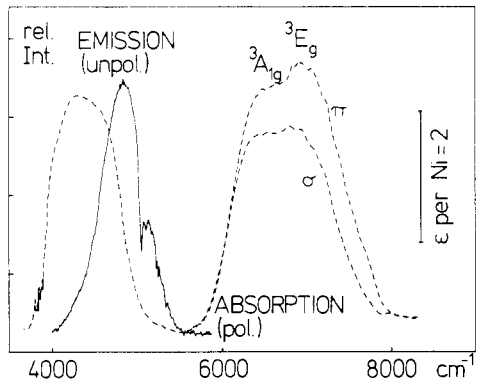


**Figure 2.** Emission spectra of $CsMg_{1-x}Ni_xBr_3$ ($x < 0.02$, $T = 18$ K, solid line) and $CsNiBr_3$ ($T = 17$ K, dashed line) and absorption spectrum of $CsNiBr_3$ (T = 12 K, dashed line).

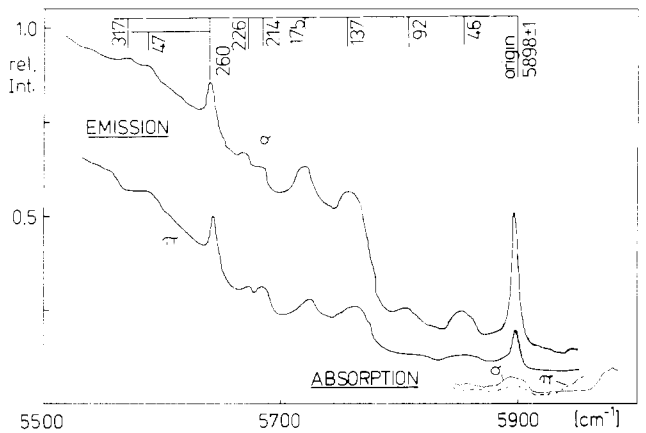


**Figure 3.** Fine structure of the $CsMg_{1-x}Ni_xCl_3$ emission and absorption bands in the origin region. The $\epsilon$ value of the origin in absorption is estimated to be 0.1 L/(mol·cm).

In the case of the concentrated materials no luminescence fine structure was observed. Sorgen et al.[11] reported and interpreted some structure on the first absorption band in $CsNiCl_3$, which we could reproduce. The luminescence bands are much broader than those of the doped samples, and their shape indicates that luminescence from more than one type of center is observed, in contrast to the diluted materials. The luminescence intensity is several orders of magnitude smaller for the extended systems than for $CsMg_{1-x}Ni_xCl_3$ and $CsMg_{1-x}Ni_xBr_3$. Within the experimental error, which is rather large for the pure compounds due to the low intensity, all the decay curves are exponential. As shown in

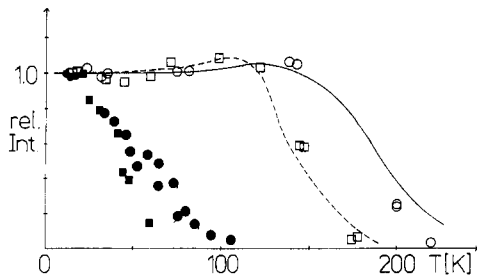


**Figure 4.** Luminescence intensity as a function of temperature for $CsMg_{1-x}Ni_xCl_3$ ($x < 0.01$, open circles), $CsNiCl_3$ (solid circles), $CsMg_{1-x}Ni_xBr_3$ ($x < 0.02$, open squares), and $CsNiBr_3$ (solid squares). The solid curves are calculated with eq 15.

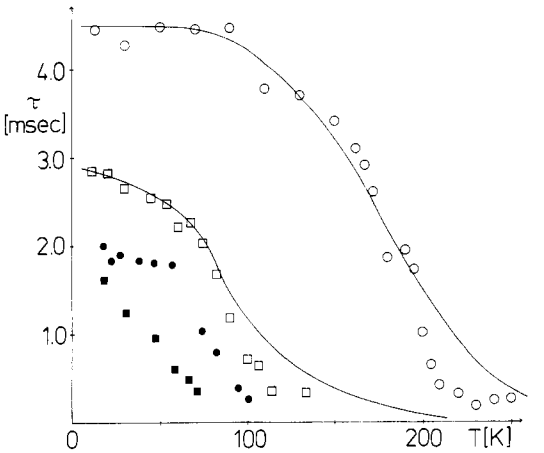


**Figure 5.** Temperature dependence of the luminescence decay times of $CsMg_{1-x}Ni_xCl_3$ ($x < 0.01$, open circles), $CsNiCl_3$ (solid circles), $CsMg_{1-x}Ni_xBr_3$ ($x < 0.01$, open squares), and $CsNiBr_3$ (solid squares). The solid curves are calculated with eq 12.

Figure 5 the 13 K decay times are of the order of a few milliseconds for the diluted compounds and are somewhat shorter in the pure materials. Their temperature dependence is comparable to the temperature dependence of the luminescence intensity. The luminescence behavior will be analyzed in sections 4.2 and 4.3.

## 4. Discussion

**4.1. Vibrational Fine Structure and Symmetry of the First Excited State.** The $Ni^{2+}$ ion is a $d^8$ system with a $^3A_{2g}$ ground state and $^3T_{2g}$ as first excited state ($O_h$ notation). The site symmetry of $Ni^{2+}$ in the present compounds is $D_{3d}$; i.e., the center of inversion is retained, and the $^3T_{2g}$ state splits into $^3A_{1g}$ and $^3E_g$. The $NiX_6^{4-}$ octahedra are slightly elongated along the trigonal axis. The purely electronic transitions to these excited states are electric dipole (ED) forbidden, but magnetic dipole (MD) allowed with the following selection rules:

$$^3A_{2g} \rightarrow {}^3A_{1g} \qquad E \perp c\ (\sigma)$$

$$^3A_{2g} \rightarrow {}^3E_g \qquad E \parallel c\ (\pi)$$

There is an intensity mechanism proposed by Herzberg and Teller[12] that provides ED intensity to a parity-forbidden electronic transition by the simultaneous excitation of an odd vibration. The appropriate factor group for this crystal structure is $D_{6h}^4$, and according to ref 13 the following 15 odd parity vibrations are obtained at $k = 0$, the center of the Brillouin zone:

$$2a_{2u} + 3e_{1u} + 2b_{1u} + b_{2u} + 2e_{2u}$$

The vibronic selection rules[13] are reproduced in Table I. We expect 7 and 10 vibronic origins for the $^3A_{1g}$ and $^3E_g$ transitions, respectively. If we turn to the experimental results, the band at 5898 cm$^{-1}$, which is observed at the same position in emission (bandwidth 10 cm$^{-1}$) and absorption, can be assigned to the purely

(11) Sorgen, A.; Cohen, E.; Makovsky, J. *Phys. Rev. B: Condens. Matter* **1974**, *10*, 4643.

(12) Herzberg, G.; Teller, E. *Z. Phys. Chem., Abt. B* **1933**, *21*, 410.

(13) Hauser, A.; Güdel, H. U. *J. Lumin.* **1982**, *27*, 249.

**Table I.** Vibronic Selection Rules for the Trigonal ($D_{3d}$) Components of the $^3A_{2g} \leftrightarrow {}^3T_{2g}$ Transition[a]

| $D^4_{6h}$ | $D_{3d}$ | transition | polarization |
|---|---|---|---|
| $a_{1u}$, $b_{1u}$ | $a_{1u}$ | $^3A_{2g} \leftrightarrow {}^3A_{1g}$ | $E \parallel c$ |
| | | $^3A_{2g} \leftrightarrow {}^3E_g$ | $E \perp c$ |
| $a_{2u}$, $b_{2u}$ | $a_{2u}$ | $^3A_{2g} \leftrightarrow {}^3A_{1g}$ | forbidden |
| | | $^3A_{2g} \leftrightarrow {}^3E_g$ | $E \perp c$ |
| $e_{1u}$, $e_{2u}$ | $e_u$ | $^3A_{2g} \leftrightarrow {}^3A_{1g}$ | $E \perp c$ |
| | | $^3A_{2g} \leftrightarrow {}^3E_g$ | $E \parallel c$, $E \perp c$ |

[a] $D^4_{6h}$ is the relevant factor group.

**Table II.** Vibrational Energies ($cm^{-1}$) in the Ground State of $CsMCl_3$ (M = Mg, Ni)

| mode | $CsMgCl_3$[a] | $CsNiCl_3$[b] | $CsMg_{1-x}Ni_xCl_3$[c] | atoms involved in normal coordinates[d] |
|---|---|---|---|---|
| $a_{1g}$ | 255[d] | 264 | 260 | Cl |
| $e^a_{1u}$ | 82 | 74 | ~92 | mainly Cs |
| $e^b_{1u}$ | 174 | 176 | 175 | mainly Cl |
| $e^c_{1u}$ | 317 | 258 | 317 | M, Cl |
| $e^a_{2u}$ | | | 46 | M, Cl |
| $e^b_{2u}$ | | | 226 | M, Cl |
| $a^a_{2u}$ | 49 | 52 | | mainly Cs |
| $a^b_{2u}$ | 250 | 192 | | M, Cl |
| $b^a_{1u}$ | | | 137 | M, Cl |
| $b^b_{1u}$ | | | 214 | M, Cl |

[a] Reference 16. [b] Reference 17. [c] This work. [d] Reference 18.

electronic transition to the lowest excited state. At 260 $cm^{-1}$ to lower energy the first member of the progression in the totally symmetrical vibration is observed. The spin–orbit splitting of the origin is smaller than the experimental bandwidth and could not be resolved. Theoretically it is calculated to be a few wavenumbers for $^3A_{1g}$.[14] The remaining fine structure can be assigned to seven ED-allowed vibronic origins with energies 46, 92, 137, 175, 214, 226, and 317 $cm^{-1}$ lower than the origin. The three $e_{1u}$ modes could easily be assigned by a comparison with existing infrared spectroscopic data.[16,17] For the other modes the dichroic ratio of the sidebands and the selection rules from Table I were used to make the assignment. Due to partial depolarization, which is extremely difficult to avoid in this type of experiment, all the sidebands are observed in both polarizations. Their intensity is larger by a factor of 1.5–3 in the polarization predicted in Table I. An analogous assignment of the sidebands was found in the isostructural compound $CsMg_{1-x}V_xCl_3$.[13] A summary of the analysis is given in Table II.

The relatively large width of the vibronic sidebands is due, in part, to contributions from vibrational functions with $k \neq 0$.[15] A nice illustration of this effect is the presence of the very broad and weak $e_{1u}{}^a$ sideband, which, according to the unit cell analysis, should not be observed in first order at $k = 0$, because Cs, but not Ni and Cl, atoms participate in this mode. Away from the zone center this selectivity is somewhat relaxed.

The symmetry of the emitting state can be deduced from the experiments in two independent ways: (i) The observed polarization of the origin where the dichroic ratio $I_\sigma/I_\pi$ of about 3 is strong evidence that the luminescent state is $^3A_{1g}$. (ii) The absence of $a_{2u}$ vibrational sidebands in the luminescence spectrum is only expected for a $^3A_{1g}$ state, as can be deduced from Table I.

This order of the trigonal components with the $^3A_{1g}$ lower than the $^3E_g$ can be rationalized with point charge or angular overlap arguments. For the calculation it is essential to include not only the six halide ions of the first coordination sphere but also the two axial magnesium ions in the second sphere. The latter make a dominant contribution to the axial ligand field potential. With

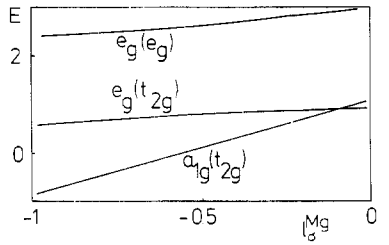


**Figure 6.** Energies of the $Ni^{2+}$ d orbitals calculated by the angular overlap model (AOM). Four AOM parameters are necessary: $l_\sigma^{halide}$, $l_\pi^{halide}$, $l_\sigma^{Mg}$, and $l_\pi^{Mg}$. In the figure the energies are given in $l_\sigma^{halide}$ units as a function of $l_\sigma^{Mg}$, varying from $l_\sigma^{Mg} = 0$ (no influence of the $Mg^{2+}$ ions) to $l_\sigma^{Mg} = -l_\sigma^{halide}$ (influence of the $Mg^{2+}$ ions equivalent in magnitude to that of the halide ions). For the remaining parameters the relations $l_\pi^{halide} = 0.25 l_\sigma^{halide}$ and $l_\pi^{Mg} = 0.3 l_\sigma^{Mg}$ were used.

the atom positions of $CsMgCl_3$ an angular overlap calculation with a reasonable set of AOM parameters according to ref 19 yields the orbital energies shown in Figure 6. The $a_{1g}$ orbital is stabilized by the interaction with the empty $3p_z$ orbitals of the $Mg^{2+}$ ions and thus becomes the most stable orbital. If, in contrast, we only consider the elongated $NiCl_6^{4-}$ octahedron, we obtain the reversed and thus incorrect orbital order. The splitting of the $^3A_{1g}$ and $^3E_g$ states is easily obtained from the one-electron energies by using the $d^8$(electrons) $\leftrightarrow$ $d^2$(holes) analogy and the Clebsch–Gordan coefficients for a trigonal basis as tabulated in ref 20:

$$\Delta E(^3E_g - {}^3A_{1g}) = \tfrac{1}{4}(\langle e_g(O_h{:}t_{2g})|V_{LF}|e_g(O_h{:}t_{2g})\rangle - \langle a_{1g}(O_h{:}t_{2g})|V_{LF}|a_{1g}(O_h{:}t_{2g})\rangle) \quad (1)$$

The experimentally observed order of the trigonal components is reproduced correctly by this simple model calculation.

It is interesting to note that for the analogous $V^{2+}$ systems about one-third of the luminescence intensity is contained in the origin and the corresponding totally symmetrical progression,[13] whereas in our case less than 10% of the emission intensity is MD.

From the intensity distribution within the totally symmetrical progression the Huang–Rhys parameter $S$ can be calculated as[21]

$$I_n = \frac{S^n}{n!}e^{-S} \quad (2)$$

with $n$ being the number of $a_{1g}$ quanta involved. From the first two members of the progression in the spectrum of $CsMg_{1-x}Ni_xCl_3$, we obtained a value of 2.5 ± 0.2 for $S$. With this the distortion along a totally symmetrical configuration coordinate $\Delta Q_{a_{1g}}$ is obtained as

$$\Delta Q_{a_{1g}} = \left(\frac{2S\hbar\omega_{a_{1g}}}{f}\right)^{1/2} \quad (3)$$

where $\Delta Q_{a_{1g}}$ is defined by

$$\Delta r = \frac{1}{6^{1/2}}\Delta Q_{a_{1g}} \quad (4)$$

For a $NiCl_6^{4-}$ octahedron, $\Delta r$ is the change in the Ni–Cl distance, $\hbar\omega_{a_{1g}}$ is the energy of the totally symmetrical vibration, and $f$ is the force constant, calculated for a harmonic oscillator. Implicit in eq 3 is the assumption that a distortion is possible only along a totally symmetrical configuration coordinate. With our value of $S$ we obtain $\Delta Q_{a_{1g}} = 0.7 \pm 0.1$ Å, which yields $\Delta r = 0.24 \pm 0.02$ Å for the change in the Ni–Cl distance. In the bromide compound the totally symmetrical progression is not resolved. We estimate the Huang–Rhys parameter from the Stokes shift[21]

$$S = \frac{\text{Stokes shift}}{2\hbar\omega_{a_{1g}}} \quad (5)$$

and obtain $S = 5.6 \pm 0.5$ for $CsMg_{1-x}Ni_xBr_3$ and, using eq 3 and 4, $\Delta r = 0.31 \pm 0.05$ Å. The distortion is larger in the bromide

(14) König, E.; Kremer, S. "Ligand Field Energy Diagrams"; Plenum Press: New York, 1977.
(15) Flint, C. D. *Coord. Chem. Rev.* **1974**, *14*, 47.
(16) McPherson, G. L.; Chang, J. R. *Inorg. Chem.* **1973**, *12*, 1196.
(17) Akiyama, K.; Morioka, Y.; Nakagawa, I. *Bull. Chem. Soc. Jpn.* **1978**, *51*, 103.
(18) Johnstone, I. W.; Jones, G.; Lockwood, D. J. *Solid State Commun.* **1981**, *39*, 395.
(19) Schäffer, C. E. *Pure Appl. Chem.* **1970**, *24*, 361.
(20) Sugano, S.; Tanabe, Y.; Kamimura, H. "Multiplets of Transition Metal Ions in Crystals"; Academic Press: New York, 1970.
(21) Wilson, R. B.; Solomon, E. I. *Inorg. Chem.* **1978**, *17*, 1729.

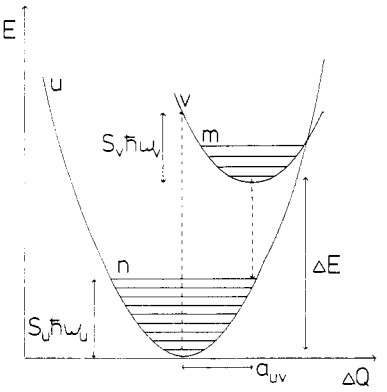


**Figure 7.** Single configuration coordinate model used to describe the temperature dependence of the decay times and luminescence intensities for the doped compounds.

than in the chloride compound. The $NiX_6^{4-}$ unit is expanded in the excited state, as the $^3A_{2g} \rightarrow {}^3T_{2g}$ transition corresponds to a $t_{2g} \rightarrow e_g$ ($O_h$ notation) orbital excitation. The expansions found in the first excited states of $VCl_6^{4-}$,[13] $Cr(NH_3)_6^{3+}$,[21] $CrCl_6^{3-}$,[22] and $Co(NH_3)_6^{2+}$ [23] are smaller by a factor of 2–3 than our $\Delta r$ values. This is consistent with the mentioned small MD contribution to the total absorption and luminescence intensity and the luminescence quenching at relatively low temperatures (in $CsMg_{1-x}V_xCl_3$ no decrease of luminescence intensity is observed below 300 K[13]), which is discussed in the following section. Even though the physical origins of these three observations are not precisely the same, all the results show that in our compounds the coupling of the electronic states of the $Ni^{2+}$ ion to the vibrating host lattice is stronger than in the other examples mentioned above.

**4.2. Relaxation Mechanisms for a $Ni^{2+}$ Center.** As can be seen from Figures 4 and 5 there is a strong temperature dependence of both the luminescence intensity and the decay time between 10 and 300 K. The quenching of the luminescence and the shortening of the decay time with increasing temperature can be attributed to radiationless deactivation, which is faster than the radiative transition. The competition of these two processes determines the observed temperature dependences. A simple model to treat this situation, the single configurational coordinate model, was first proposed by Huang and Rhys[24] and further developed by Struck and Fonger.[25] We apply this model to our situation as follows.

The electronic transition is treated in terms of two transition rates, the radiative rate $W_R$ and the nonradiative rate $W_{NR}$. These rates determine the quantum efficiency $\eta$ and the decay time $\tau$

$$\eta = \frac{W_R}{W_R + W_{NR}} = \frac{\tau}{\tau_R} \tag{6}$$

and

$$\frac{1}{\tau} = \frac{1}{\tau_R} + \frac{1}{\tau_{NR}} \tag{7}$$

where $\tau_R$ is the purely radiative decay time.

The goal is to calculate $W_R$ and $W_{NR}$ as functions of temperature by using experimentally available information. In the model we assume harmonic potentials for the ground and the first excited electronic states, which are shifted along a configurational coordinate, as can be seen from Figure 7, where all the important quantities are introduced.

The probability for a transition from level $v_m$ to level $u_n$ can be written for the radiative process as

$$R_{nm} = R_{uv}(1 - r_v)r_v^m\langle u_n|v_m\rangle^2 \tag{8}$$

and analogously for the radiationless case as

$$N_{nm} = N_{uv}(1 - r_v)r_v^m\langle u_n|v_m\rangle^2 \tag{9}$$

**Table III.** Parameter Values for the Configuration–Coordinate Model Calculation (according to Figure 7)

| parameter | $CsMg_{1-x}Ni_xCl_3$ | $CsMg_{1-x}Ni_xBr_3$ |
|---|---|---|
| $\tau_R$, ms | 5.2 | 3.2 |
| $\hbar\omega_u$, $cm^{-1}$ | 260 | 193 |
| $\hbar\omega_u/\hbar\omega_v$ | 1 | 1 |
| $\theta$, rad | 0.785 | 0.785 |
| Stokes shift,[a] $cm^{-1}$ | 1800 | 2150 |
| $a_{uv}$ | 3.72 | 4.73 |
| $\Delta E$, $cm^{-1}$ | 5898 | 5500 |
| $p_U$ | 23 | 28 |

[a] $T$ = 18 K.

where $r_v = \exp(-\hbar\omega_v/kT)$ determines the thermal weight and $N_{uv}$ and $R_{uv}$ are the purely electronic parts of the transition moments. The latter two parameters are assumed to be constant in this model, thus neglecting the interstate vibronic coupling. According to ref 26 this approximation is not critical in cases similar to the present one.

The total rates are obtained by summing over all the possible initial and final vibrational states for a given electronic transition. For the radiative process the products of thermal weight and the Franck–Condon factor form a normalized distribution, so that the total rate $W_R$ turns out to be temperature independent.

For the radiationless deactivation the following energy relationship must hold, as can easily be seen from Figure 7:

$$\Delta E + m\hbar\omega_v - n\hbar\omega_u = 0 \quad \text{for } v_m \rightarrow u_n \tag{10}$$

The sum over all possible $v_m$ and $u_n$ will thus be smaller than $N_{uv}$, and the total radiationless rate becomes temperature dependent because of the $r_v$ factors. By several steps of algebra the nonradiative rate $W_{NR}$ for a transition is obtained as[25]

$$W_{NR} = N_{uv}\sum_{m=m_0}^{\infty}(1 - r_v)r_v^m\langle u_{p_U+m}|v_m\rangle^2 \tag{11}$$

where $p_U$ is the number of phonons required to bridge the energy difference $\Delta E$, $m_0$ is the larger value of 0 and $-p_U$, and the potentials for the ground and excited state are assumed to have the same shape, i.e. $\hbar\omega_v = \hbar\omega_u$. Finally the decay time of the luminescence can be written as

$$\frac{1}{\tau} = \frac{1}{\tau_R} + W_{NR} \tag{12}$$

In the actual calculation we used $\tau_R$ as well as the vibrational frequency $\hbar\omega_u$ as adjustable parameters. For $N_{uv}$ a value of $10^{13}$ $s^{-1}$ was taken from ref 25. According to ref 27 this value can be considered as typical for a variety of host lattices. The Franck–Condon factors can be calculated by using Manneback's recursion formulas,[25] the vibrational energy $\hbar\omega_u$ and the experimental Stokes shift. The result of a least-squares fit to the measured decay times is shown in Figure 5. The corresponding parameter values are collected in Table III.

The experimental decay times are well described by the calculated curves. A deviation for both compounds is observed at higher tempertatures. This is most likely due to the fact that the model considers only a single accepting mode. The theoretical values for the decay times are thus probably too high. The purely radiative lifetimes $\tau_R$ are higher than the observed low-temperature values of $\tau$ for both compounds, the differences being 16% for the chloride and 30% for the bromide. The nonradiative deactivation is already efficient at 13 K in these compounds. In fluoride lattices, on the other hand, the nonradiative relaxation appears to be negligible at 10 K according to measurements on $Mg_{1-x}Ni_xF_2$.[28] As a check, the radiative lifetime can be deter-

(22) Snellgrove, T.; Güdel, H. U. *Inorg. Chem.* **1978**, *17*, 1617.
(23) Wilson, R. B.; Solomon, E. I. *J. Am. Chem. Soc.* **1980**, *102*, 4085.
(24) Huang, K.; Rhys, A. *Proc. R. Soc. London, A* **1950**, *204*, 406.
(25) Struck, C. W.; Fonger, W. H. *J. Lumin.* **1975**, *10*, 1.
(26) Blasse, G. In "Radiationless Processes"; Di Bartolo, B., Ed.; Plenum Press: New York, 1979; NATO ASI Ser., Ser. B62.
(27) Van Dijk, J. M. F.; Schuurmans, M. F. H. *J. Chem. Phys.* **1983**, *78*, 5317.
(28) Vehse, W. E.; Lee, K. H.; Yun, S. J.; Sibley, W. A. *J. Lumin.* **1975**, *10*, 149.

mined from the oscillator strength of the corresponding transition in absorption with

$$f\tau_R = 1.5 \times 10^4 \left(\frac{\lambda_0^2}{n^3}\right) \quad \text{(SI units}^{29}\text{)} \qquad (13)$$

where $f$ is the experimentally determined oscillator strength, $\lambda_0$ the wavelength of the absorption maximum and $n$ the refractive index. With reasonable values for $CsMg_{1-x}Ni_xCl_3$, $\lambda_0 = 1500$ nm, $n = 1.6$, and $f = 2 \times 10^{-6}$ (at 13K), $\tau_R = 4$ ms is obtained, a value that is in satisfactory agreement with the $\tau_R$ value of 5.2 ms resulting from the fit to the decay times. From the measured increase of the oscillator strength with temperature, enabling-mode energies of 356 and 222 $cm^{-1}$ were determined for the diluted chloride and bromide crystals, respectively. According to eq 13 this leads to a decrease of $\tau_R$ of 6% between 10 and 150 K and of 9% between 10 and 100 K for these compounds, which was neglected in our model calculation.

$Ni^{2+}$ centers in $MgF_2$,[8] $KMgF_3$,[28] and MgO[28] show two luminescence bands in the green and red spectral regions in addition to the $^3T_{2g} \rightarrow {}^3A_{2g}$ IR emission. These unusual high-energy bands correspond to $^1T_{2g} \rightarrow {}^3A_{2g}$ and $^1T_{2g} \rightarrow {}^3T_{2g}$ transitions. We searched very carefully but in vain for the corresponding transitions in $CsMgCl_3$ and $CsMgBr_3$. The nonradiative deactivation of the $^1T_{2g}$ state is obviously more competitive in these materials than in the fluoride and oxide lattices. This is in good correspondence with our conclusions about the deactivation of the $^3T_{2g}$ state.

The fitted vibrational energies $\hbar\omega_u$ give the right order of magnitude for both compounds. In $CsMg_{1-x}Ni_xCl_3$, $\hbar\omega_u$ is identical with the $a_{1g}$ vibrational energy determined from the vibronic fine structure in the preceding section. It is expected that in the present systems a shift of the parabolic potentials can only occur along a totally symmetrical configurational coordinate, so this is a satisfactory result. No Raman data are available for the bromide, but we can estimate $\hbar\omega_{a_{1g}}$ with the following equation:[30]

$$\frac{\hbar\omega_{a_{1g},Ni-Cl}}{\hbar\omega_{a_{1g},Ni-Br}} = \left(\frac{f_{Ni-Cl}}{f_{Ni-Br}}\right)^{1/2}\left(\frac{m_{Br}}{m_{Cl}}\right)^{1/2} \qquad (14)$$

The ratio of the force constants is known to be 1.16 for the analogous $V^{2+}$ compounds.[31] Since the $a_{1g}$ mode involves only motions of the halide ions, this value can be used for the $Ni^{2+}$ compounds as well, and we obtain an estimated $a_{1g}$ energy of 180 $cm^{-1}$ for $CsMg_{1-x}Ni_xBr_3$, which agrees well with the $\hbar\omega_u$ value of 193 $cm^{-1}$ resulting from the Struck and Fonger model.

The luminescence intensities for both doped compounds show qualitatively the same temperature behavior as the decay times, but the luminescence quenching occurs at higher temperatures than the shortening of the decay times. We explain this with the temperature dependence of the broad-band excitation efficiency, i.e. the temperature dependence of the highest energy d–d and the lowest energy charge-transfer absorption bands. Assuming a vibronic intensity mechanism for the parity forbidden transitions, the following expression for the relative luminescence intensity as a function of temperature is obtained:

$$\frac{I(T)}{I(T=0)} = \frac{\tau}{\tau_R} \coth\left(\frac{\hbar\omega}{2kT}\right) \qquad (15)$$

with $\tau/\tau_R$ resulting from the analysis of the decay time measurements and the coth factor describing the intensity of the absorption bands in which the excitation occurs. The vibrational energy $\hbar\omega$ is an overall enabling mode and is treated as an adjustable parameter. The resulting values from least-squares fits to the experimental intensities, 279 $cm^{-1}$ for the chloride and 137 $cm^{-1}$ for the bromide, are not very meaningful as absolute numbers because various ungerade vibrations can be involved, but they do

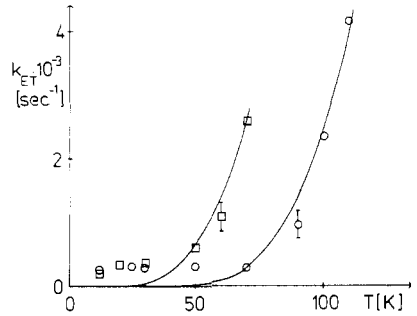


**Figure 8.** Energy transfer rate $k_{ET}$ as a function of temperature for $CsNiCl_3$ (circles) and $CsNiBr_3$ (squares) with theoretical curves according to eq 17.

**Table IV.** Activation Energy for Radiationless Energy Transfer ($\Delta E$) and Transfer Rate $k_{ET}$ at $T \rightarrow \infty$

| compd | $\Delta E$, $cm^{-1}$ | $k(T \rightarrow \infty)$, $s^{-1}$ |
|---|---|---|
| $CsNiCl_3$ | 360 ± 30 | $4.4 \times 10^5$ |
| $CsNiBr_3$ | 170 ± 45 | $4.0 \times 10^4$ |

give the right order of magnitude for Ni–X vibrational energies in the present lattices. The experimental intensities together with the calculated curves (according to eq 15) are shown in Figure 4. In view of the simplifications of the model the agreement is good.

The temperature dependence of luminescence intensities and decay times has enabled us to obtain a detailed and consistent picture of the dominant relaxation processes in the lowest energy excited state of $Ni^{2+}$ centers in $CsMgCl_3$ and $CsMgBr_3$. Decay time measurements have yielded more quantitative information than intensity measurements.

**4.3. Transfer of Excitation Energy in $CsNiCl_3$ and $CsNiBr_3$.** The phenomenon of radiationless transfer of excitation energy in extended systems of exchange-coupled transition-metal ions is well-known.[32] The luminescence properties in the concentrated compounds $CsNiCl_3$ and $CsNiBr_3$ are governed by such energy-transfer processes. They are not comparable with the behavior of the diluted systems discussed in the preceding section, where the excitation was localized on one center. Immediate evidence for this is provided by the short decay times in the concentrated materials as well as the estimated absolute luminescence intensities, which are several orders of magnitude smaller for the pure than for the doped compounds. The observed bandwidths and band shapes indicate that luminescence from different kinds of centers, e.g. $Ni^{2+}$ ions at lattice defects or unintentional impurities, is observed. $Co^{2+}$ could act as an efficient luminescent trap in the present systems, because its lowest energy absorption band[33] overlaps strongly with the nickel luminescence, so that the activation barrier for $Ni^{2+} \rightarrow Co^{2+}$ transfer should be small. We interpret the quenching of the luminescence intensities and decay times in the concentrated materials as a result of energy transfer to unidentified killer traps in the lattice. The relative luminescence intensities do not allow any quantitative conclusions about the energy transfer. From the decay time behavior, on the other hand, it is possible to derive a macroscopic rate for the energy transfer from the $Ni^{2+}$ system to the killer traps. It is given by[32]

$$k_{ET} = \tau_s^{-1} - (\tau_s^\circ)^{-1} \qquad (16)$$

where $\tau_s$ and $\tau_s^\circ$ are the deactivation times of the $Ni^{2+}$ system, with and without energy transfer to killer traps, respectively. From the doped and the pure samples we have all the data to determine $k_{ET}$ as a function of temperature. Empirically, its temperature dependence can be described with an activation law

$$k_{ET}(T) = k_{ET}(T \rightarrow \infty)\, e^{-\Delta E/k_B T} \qquad (17)$$

with $\Delta E$ as an activation energy for the transfer process.

(29) Imbusch, G. F. In "Luminescence Spectroscopy"; Lumb, M., Ed.; Academic Press: New York, 1978.
(30) Nakamoto, K. "Infrared Spectra of Inorganic and Coordination Compounds"; Wiley: New York, 1963.
(31) Hauser, A. Ph.D. Thesis, Universität Bern, 1983.
(32) Powell, R. C.; Blasse, G. *Struct. Bonding (Berlin)* **1980**, *42*, 43.
(33) Putnik, S.; Holt, S. L. *Inorg. Chem.* **1977**, *16*, 1010.

Plots of $k_{ET}$ vs. $T$ are shown in Figure 8. At high temperatures a more or less exponential relationship is observed. The values for $k_{ET}$ ($T \rightarrow \infty$) and $\Delta E$, determined from this region, are contained in Table IV. They have to be considered as a lower limit to the true activation energy. The reason for the deviations from an Arrhenius type behavior at low temperatures lies in the dominance of alternative processes with very low activation barriers. One likely possibility are transfer processes to the killer traps from their near $Ni^{2+}$ neighbors. The overall transfer rate $k_{ET}$ from the nickel system to the quenching traps may be limited by the individual $Ni^{2+} \rightarrow Ni^{2+}$ steps, i.e. diffusion within the $Ni^{2+}$ system, or the trapping step may be limiting. Our data do not allow a clear assignment to one of these limiting cases, because the nature of the killer traps is not known. However, an activation barrier is expected for the $Ni^{2+} \rightarrow Ni^{2+}$ step on several grounds. Resonant energy transfer depends on the spectral overlap between the donor emission and acceptor absorption bands. As a result of the geometrical expansion in the relaxed excited state and the concomitant Stokes shift, only the very weak electronic origins contribute to the spectral overlap below 10 K. This would be the most obvious reason for a thermal activation of the $Ni^{2+} \rightarrow Ni^{2+}$ transfer. In antiferromagnetically ordered materials, and there are antiferromagnetic correlations along the chains in $CsNiX_3$ type compounds up to high temperatures,[34] there is an additional barrier. Excitation transfer between nearest neighbors is doubly spin-forbidden. This can be overcome by magnon-assisted processes, which require finite magnon populations and thus lead to a thermal activation. Finally, the trigonal $^3E_g$ ($T_{2g}$) component may be highly more efficient to promote purely excitonic energy transfer than $^3A_{1g}$ ($T_{2g}$), which again would lead to a thermally activated process. This mechanism was recently postulated to be mainly responsible for the energy-transfer behavior in several antiferromagnetic $Mn^{2+}$ compounds.[35] The observed activation energies in $CsNiCl_3$ and $CsNiBr_3$ are similar in magnitude to those determined in $[(CH_3)_4N]MnCl_3$,[36] $RbMnCl_3$, and $CsMnBr_3$.[35] Relaxation in the excited state and transfer via a high-energy exciton are both likely mechanisms for the observed thermal barriers in the $Ni^{2+}$ systems.

**Acknowledgment.** We thank H. Riesen for helpful discussions. Financial support by the Swiss National Science Foundation is gratefully acknowledged.

**Registry No.** $CsNiCl_3$, 15455-69-3; $CsNiBr_3$, 15455-70-6.

(34) Ueda, K.; Tanabe, Y. *J. Phys. Soc. Jpn.* **1980**, *48*, 1137.
(35) Kambli, U.; Güdel, H. U. *Inorg. Chem.* **1984**, *23*, 3479.
(36) Yamamoto, H.; McClure, D. S.; Marzzacco, C.; Waldman, M. *Chem. Phys.* **1977**, *22*, 79.

Contribution from the Departments of Chemistry, Ben Gurion University, Beer Sheva 84120, Israel, and North Carolina State University, Raleigh, North Carolina 27695-8204

# Electronic and Intramolecular Structural Localizations in Conducting Organic Salts

Sason S. Shaik*[†] and Myung-Hwan Whangbo*[‡]

*Received June 24, 1985*

We examined the energy factors governing intramolecular structural localization, which leads to a mixed-valence structure for molecular stacks and hence to a $4k_f$ CDW in small-$U$ limit (i.e., $U/4|\beta| < 1$). Intramolecular structural localization is found to occur when $E_R/4|\beta| > 1$, where the intramolecular relaxation energy $E_R$ is a measure of the tendency for a stacking molecule to relax its geometry upon losing or gaining an electron. For a donor stack $E_R$ is found to be approximated by $2(IP^v - IP^a)$, given the vertical and adiabatic ionization potentials of the donor as $IP^v$ and $IP^a$, respectively. On the basis of these ionization potentials and the estimates of bandwidth $4|\beta|$, the intramolecular structural localization condition was tested for several well-studied organic salts. For a donor molecule, the tendency for intramolecular relaxation is found to increase as antibonding character of its HOMO increases. Thus, sulfur-based donor molecules have a stronger tendency for intramolecular relaxation than do their selenium analogues, which appears to be why a $4k_f$ CDW is more likely to be found from sulfur-based donors. To examine how electronic localization (i.e., $U/4|\beta| > 1$) and intramolecular structural localization (i.e., $E_R/4|\beta| > 1$) affect the electronic structures of molecular stack, we performed band electronic structure calculations on several mono-valence and mixed-valence structures of $TTF^{1/2+}$ and $TTF^{2/3+}$ stacks. Analysis of these results led us to formulate simple models of $2k_f$ and $4k_f$ CDW's in terms of intramolecular and intermolecular distortions.

In the past decade, conducting organic salts have been synthesized from various donor and acceptor molecules (e.g., see Chart I).[1] Invariably, these organic metals contain stacks of partially oxidized donor molecules D and/or stacks of partially reduced acceptor molecules A. In average, each molecule of a donor or an acceptor stack may be regarded as carrying a fractional charge $\rho$. For example, $(TMTSF)_2X$ ($X^- = PF_6^-$, $ClO_4^-$, etc.) is characterized by $TMTSF^{0.5+}$, TTF·TCNQ by $TTF^{0.59+}$ and $TCNQ^{0.59-}$, TSF·TCNQ by $TSF^{0.63+}$ and $TCNQ^{0.63-}$, and $(TTF)_3(BF_4)_2$ by $TTF^{2/3+}$. Many of these organic salts have a metallic conductivity at room temperature but become insulators at lower temperatures owing to some *localization* and *distortion mechanisms* that pin the electrons and restrict their mobility.

Two different mechanisms are generally considered to be responsible for metal–insulator transitions in molecular stacks. One mechanism is a Peierls distortion.[2] In general, a uniform molecular stack with a partially filled metallic band is susceptible to a structural distortion that opens a band gap at the Fermi level. If the band filling is $f$ or $1 - f$ ($0 < f \leq {}^1/_2$), the uniform stack will distort to one in which the unit cell size becomes $1/f$ times as large as that of the uniform stack. An example for such a

**Chart I**

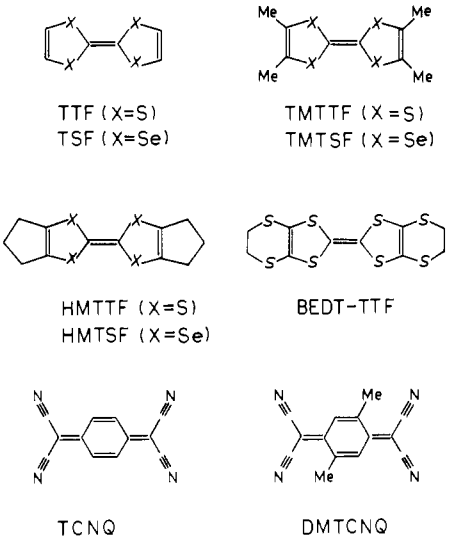


[†] Ben Gurion University.
[‡] Camille and Henry Dreyfus Teacher-Scholar (1980–1985). North Carolina State University.

0020-1669/86/1325-1201$01.50/0 